Tortuosity-porosity relation in porous media flow

Article *in* Physical Review E · September 2008

DOI: 10.1103/PhysRevE.78.026306 · Source: PubMed

3 authors, including:

Maciej Matyka
University of Wroclaw
41 PUBLICATIONS **729** CITATIONS

SEE PROFILE

Zbigniew Koza
University of Wroclaw
60 PUBLICATIONS **1,994** CITATIONS

SEE PROFILE

Tortuosity–porosity relation in the porous media flow

Maciej Matyka,[1] Arzhang Khalili,[2,3] and Zbigniew Koza[1]

[1] *Institute of Theoretical Physics, University of Wrocław, pl. M. Borna 9, 50-204 Wrocław, Poland*
[2] *Max Planck Institute for Marine Microbiology, Celsiusstrasse 1, D-28359 Bremen, Germany*
[3] *Jacobs University Bremen, Campus Ring 1, D-28759 Bremen, Germany*

(Dated: February 2, 2008)

We study numerically the tortuosity–porosity relation in a microscopic model of a porous medium arranged as a collectin of freely overlapping squares. It is demonstrated that the finite-size effects and the discretization errors, which were ignored in previous studies, may cause significant underestimation of tortuosity. The simple tortuosity calculation method proposed here eliminates the need for using complicated, weighted averages. The numerical results presented here are in good agreement with an empirical relation between tortuosity (T) and porosity (ϕ) given by $T-1 \propto \ln\phi$, that was found by others experimentally in granule packings and sediments. This relation can be also written as $T-1 \propto RS/\phi$ with R and S denoting the hydraulic radius of granules and the specific surface area, respectively.

PACS numbers: 47.56.+r,47.15.G-,91.60.Np

I. INTRODUCTION

In the low Reynolds number regime, flow through a porous matrix is governed by Darcy's law that links the fluid flux (discharge per unit area) $\boldsymbol{q}$ with the applied pressure gradient $\boldsymbol{\nabla} P$ by the linear relation

$$\boldsymbol{q} = -\frac{k}{\mu}\boldsymbol{\nabla} P, \tag{1}$$

where μ is the dynamic viscosity of the fluid and k is a proportionality constant known as permeability [1]. To a large extent, the proper description of the fluid flow through a porous medium depends on precise relations between the physical properties involved such as permeability and porosity (ϕ). In particular, much attention has been paid to deriving relations between k and ϕ [2]. In 1927 Kozeny developed a simple capillary model for a porous medium, and proposed the relation

$$k = c_0\frac{\phi^3}{S^2}, \tag{2}$$

where S is the specific surface area and c_0 is a dimensionless Kozeny constant that depends on the channel geometry [1]. Unfortunately, Kozeny's formula is not universal and does not hold for complicated porous geometries [1]. For example, it does not take into account pore connectivity and the fact that the specific surface area can be increased to an arbitrarily large value by removing some of the material to roughen the porous matrix surface in a fractal-like manner. On a purely physical ground namely, one would expect that removal of the material from a porous matrix would increase its permeability, whereas Kozeny's formula predicts just the opposite [3].

One of the most widely accepted attempts to generalize relation (2) was proposed by Carman [1, 4, 5], who noticed that the streamlines in a porous medium are far from being completely straight and parallel to each other. This effect can be described by a dimensionless parameter T called *hydraulic tortuosity*,

$$T = \frac{\langle\lambda\rangle}{L}, \tag{3}$$

where $\langle\lambda\rangle$ is the average length of the fluid paths and L is the geometrical length of the sample [1]. Using the tortuosity, Kozeny's relation (3) can be generalized to

$$k = c_0\frac{\phi^3}{T^2S^2}. \tag{4}$$

By fitting experimental data, Carman concluded that T^2 is a constant factor ($\approx 5/2$) over a wide range of porosities. Later it was found that T^2 does vary with ϕ, and can be as large as 50 for low porosity media [6, 7].

Furthermore, it was realized that elongation of streamlines not only affects the hydraulic discharge, but also mediates other types of transport phenomena in the porous medium. This resulted in introducing several distinctive, experimentally measurable tortuosities obtained from a particular transport process, leading to diffusive [8, 9], electrical [9, 10, 11] and acoustic [11] tortuosity definitions. There were also further theoretical attempts to define tortuosity [1, 5, 12]. However, all these tortuosities, in general, differ from each other. Except for some very simple models [5, 6, 13], there is no clear consensus on the relation between these definitions. Among all these definitions, the one expressed in Eq. (3) is not only the simplest, but also widely adopted in theoretical studies, for it ties tortuosity with the underlying geometry and topology of the porous medium.

It has been known since long that flow through a porous medium depends on many factors such as porosity, tortuosity, granule shape and size distribution, saturation, Reynolds number, etc. For proper understanding of transport phenomena in porous media, however, it is essential to depart from simple systems with a limited number of well-defined control parameters. Therefore,

in this paper we investigate the hydraulic tortuosity (as defined in Eq. (3)) in a creeping flow through a porous region constructed by a two-dimensional lattice system with a uniform, randomly distributed and freely overlapping solid squares. This model, first used by Koponen *et al.* [12], is simple enough to allow a numerical solution with the advantage of having porosity (ϕ) as the only control parameter. It is particularly suitable for studying tortuosity-porosity relation, as at high porosities the streamlines are almost straight, whereas for low porosities they become wiggly.

Using the Lattice Gas Automata (LGA) method, Koponen *et al.* [12] solved the flow equations for a porosity range of $\phi \in [0.5, 1]$, and concluded that

$$T = p(1-\phi) + 1, \tag{5}$$

where p is a fitting parameter. However, later they found the relation not being consistent with the results obtained for the porosity range $\phi \in [0.4, 0.5]$, and suggested [14] to replace relation (5) by

$$T = p\frac{(1-\phi)}{(\phi-\phi_c)^m} + 1, \tag{6}$$

in which $\phi_c \approx 0.33$ is the percolation threshold while p and m are some empirical parameters. Still, as an *ad hoc* formula with two fitting parameters, this relation can not be considered a universal law. In addition, the data used to derive (6) suffer from systematic errors, as neither the impact of a finite system size nor the effect of the space discretization were taken into account.

The aim of this paper is to cary out a numerical simulation for analysing the tortuosity—porosity relation in a system of freely overlapping rectangles with a high accuracy. In addition, we provide a simplified algorithm for T calculation without the need for implementing complicated, weighted averages of streamline lengths.

The structure of the paper is as follows. Section II specifies the model and the numerical techniques used. Special attention is paid to the description of the nontrivial numerical technique for the tortuosity. Main results, including a detailed numerical error and finite-size analysis are provided in Sec. III. Finally, the results are discussed in Sec. IV.

II. MODEL

A. General description

The system of interest consists of a square lattice ($L \times L$) in which a number of solid squares ($a \times a$ lattice units) have been placed at random locations to form a porous matrix ($1 \leq a \ll L$). The squares are fixed in space but free to overlap. The only restriction is that their sides must coincide with the underlying lattice. The remaining, void space is filled with a liquid. The constant, external force imposed on the porous medium is aligned with the y-axis of an x-y Cartesian coordinate system to model the gravity. Following previous works [12, 14], periodic boundary conditions have been imposed in both directions.

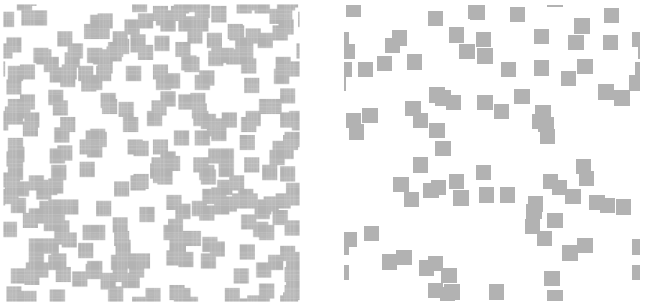

a) $\phi = 0.5$ b) $\phi = 0.8$

FIG. 1: An example of two 800×800 porous matrices constructed by randomly placed and freely overlapping rectangles of size 10×10 for two different porosities ϕ.

Two examples of such porous systems are depicted in Fig. 1. The dark areas represent fixed solid obstacles, while the white part is occupied by the fluid.

B. Numerical techniques

Numerical solution of the model defined above consists of five main steps: (i) generation of a porous matrix of a known porosity; (ii) solving the flow equations in the low Reynolds number regime; (iii) finding the flow streamlines; (iv) determining the tortuosity of the flow; (v) error analysis.

1. Construction of the porous matrix

A porous matrix of a given porosity ϕ can be generated using the method of [12, 14]. Starting from an empty system, solid squares are added at random positions until the desired porosity has been reached. The porosity is calculated as the fraction of unoccupied lattice nodes.

2. Lattice Boltzmann method for solving flow equations

To solve the flow equations, we applied the Lattice Boltzmann Model (LBM) [15] with a single relaxation time collision operator [16]. This method proved useful in microscopic model simulations of flow through porous media for various conditions and flow regimes [2, 17]. It is a numerical technique that rests on the Boltzmann transport equation discretized both in time and space, and is expressed in terms of the velocity distribution functions n_i in the form

$$n_i^{t+1}(\boldsymbol{r} + \boldsymbol{c}_i) = n_i^t(\boldsymbol{r}) + \Delta_i^t(\boldsymbol{r}) + F_i, \tag{7}$$

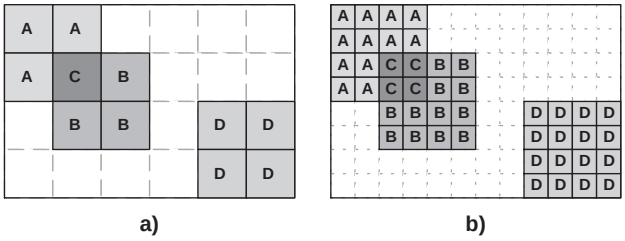

FIG. 2: A schematic view of the system before (a) and after (b) grid refinement. In this example the system size is 4×6, the porous matrix is made of three quads of size 2×2 (A, B and D), and the refinement level $k_{\rm ref} = 2$.

where $i = 0, \ldots, 8$ identifies lattice vectors $\boldsymbol{c}_i$, t is an integer time step, $\boldsymbol{r}$ denotes a lattice node, $\Delta_i^t(\boldsymbol{r})$ is the collision operator at $\boldsymbol{r}$, and F_i represents the i-th component of the external force. We used the time unit equal to the relaxation time, which yields the kinematic viscosity $\nu = 1/6$ [15]. This, in turn, simplifies the form of the collision operator $\Delta_i^t(\boldsymbol{r}) = n_i^{\rm eq}(\boldsymbol{r}) - n_i^t(\boldsymbol{r})$ with $n_i^{\rm eq}(\boldsymbol{r})$ being the equilibrium value of n_i at $\boldsymbol{r}$. The external force was taken into account using a method of Ref. [18]: half of the momentum was transferred directly into the equilibrium distribution function during the collision step, whereas the other half was included into the transport equation. Because we were interested in the solution of a slow, laminar flow, we utilized the equilibrium distribution function $n_i^{\rm eq}$ linearized in the velocity as

$$n_i^{\rm eq} = w_i \rho \left[1 + 3(\boldsymbol{u} \cdot \boldsymbol{c}_i)\right], \tag{8}$$

in which $\boldsymbol{u}$ is the macroscopic velocity vector and w_i are some weighting coefficients that depend on the lattice structure and dimension [19, 20].

One problem with the LBM method is that it is incapable of resolving the macroscopic Navier-Stokes equations for channels narrower than about 4 lattice units [15]. This limitation becomes particularly important at low porosities, for which the number of very narrow passages increase enormously. To bypass this problem, a standard numerical mesh refinement procedure was used. Starting from the original lattice taken to generate the porous matrix, each of its L^2 elementary quads were subdivided into $k_{\rm ref} \times k_{\rm ref}$ smaller quads with $k_{\rm ref} = 1, 2, \ldots$ being the refinement level. The resulting $k_{\rm ref}L \times k_{\rm ref}L$ computational grid of vectors $\boldsymbol{r}$ in Eq. (7) will then be formed from the centers of the small quads. With this choice, the identification of the interface between the porous matrix and the free space is facilitated.

A schematic picture of the refinement procedure is shown in Fig. 2. Note that the refinement effectively increases the number of the lattice nodes between any two points by the factor $k_{\rm ref}$, and that the smallest channel width is $k_{\rm ref} + 1$ lattice units.

After initialization, the LBM computational loop of advection and collision continued for 5×10^3 time steps. By using the mid-grid bounce-back rule applied to the no-slip boundaries, second order accurate solutions, both in space and time, could be achieved [15]. An example of the velocity field calculated with this method for a low-porosity medium is shown in Fig. 3.

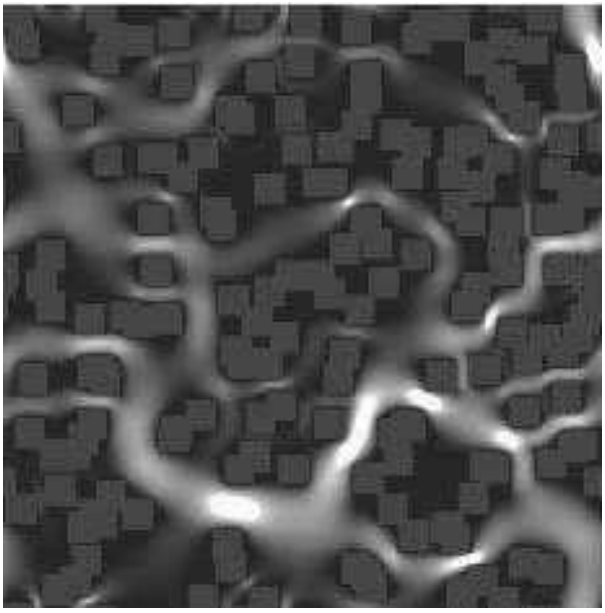

FIG. 3: Velocity magnitudes squared ($u^2 = u_x^2 + v_y^2$) calculated on a 600×600 numerical grids, which corresponds to a 200×200 lattice (refinement level $k_{\rm ref} = 3$). The square block sizes were 10×10 (i.e., 30×30 after refinement) and the porosity was $\phi = 0.65$. Periodic boundary conditions were assumed in both directions. The grey squares in the figure represent the solid part of the medium, whereas the black region is the porespace open to fluid flow.

3. Flow streamlines

After obtaining the velocity field $\boldsymbol{u}$ at each grid point, streamlines could be obtained by solving the equation of motion for the trajectories $\boldsymbol{r}(t)$ of massless particles [21],

$$\frac{d\boldsymbol{r}}{dt} = \boldsymbol{u}(\boldsymbol{r}). \tag{9}$$

The $\boldsymbol{u}(\boldsymbol{r})$ values of points lying between two grid nodes were obtained using bilinear interpolation. Due to complex boundary conditions and extreme velocity differences on the grid, the 4-th order Runge-Kutta algorithm with adaptive time stepping was used [22].

4. Tortousity

The tortuosity is defined by Eq. (3) as the ratio of the average length of all particle path lines passing through a given cross-section during a unit time period to the width

of the sample [1] leading to

$$T = \frac{1}{L}\frac{\int_A u_y(x)\lambda(x)dx}{\int_A u_y(x)dx}, \tag{10}$$

in which A is an arbitrary cross-section of the system parallel to the x axis, $\lambda(x)$ is the length of the streamline cutting A at x, and $u_y(x)$ is the y component of the trial particle velocity at x.

The integrals in (10) have been obtained in the literature either by the Monte Carlo integration [12, 14, 23] or by direct quadratures [6]. In the former method, the lengths of the streamlines passing through randomly chosen points within the pore volume are averaged using proper weights. In the latter method T is approximated by the relation

$$T \approx \frac{1}{L}\frac{\sum_j u_y(x_j)\lambda(x_j)\Delta x_j}{\sum_j u_y(x_j)\Delta x_j}, \tag{11}$$

where $\Delta x_j = x_{j+1} - x_j$ are discretization intervals of A. In principle, both approaches should yield the same results, but both can be easily misused. For example, some researchers used the Monte Carlo integration with streamlines passing through points chosen randomly from a uniform distribution over the whole pore space [12, 23], some others calculated streamlines cutting all lattice nodes [14], whereas others recorded all streamlines crossing every lattice node along a chosen inlet plane [6, 13]. However, such 'uniform' approaches are not coherent with the reality of low porosity systems, in which transport is mostly carried out only through few 'conducting' channels (cf. Fig. 3). Consequently, the sums in (11) contain most probably many terms of practically negligible magnitudes. To avoid this problem, we used Eq. (11) with a constant-flux constraint between two neighboring streamlines,

$$u_y(x_j)\Delta x_j = \text{const.} \tag{12}$$

With this choice, Eq. (11) immediately simplifies to

$$T \approx \frac{1}{L}\frac{1}{N}\sum_{j=1}^{N}\lambda(x_j), \tag{13}$$

where N is the number of the streamlines generated. Note that all terms in this sum are of the same order of magnitude.

Thus, to calculate T, a horizontal cross-section A is chosen. Next, the coordinates of the initial points x_j are determined using (12), and the corresponding streamlines are found by solving (9) in both directions until the solutions hit the system edges ($y = 0$ and $y = L$). Finally their lengths are plugged into (13).

It should be noted that not all streamlines passing through x_j cut both horizontal edges $y = 0$ and $y = L$ (see Fig. 4). This may happen if a streamline passes through a region with extremely low fluid velocity. There are two types of such regions: dead-end pores and volumes where the fluid stream is split by an obstacle (or merges behind it). An example of x_j located in a dead-end pore is shown by arrow (a) in Fig. 4. Arrow (b) points at x_j corresponding to an incomplete streamline that flows from a region (c) where the stream merges after being split by an obstacle.

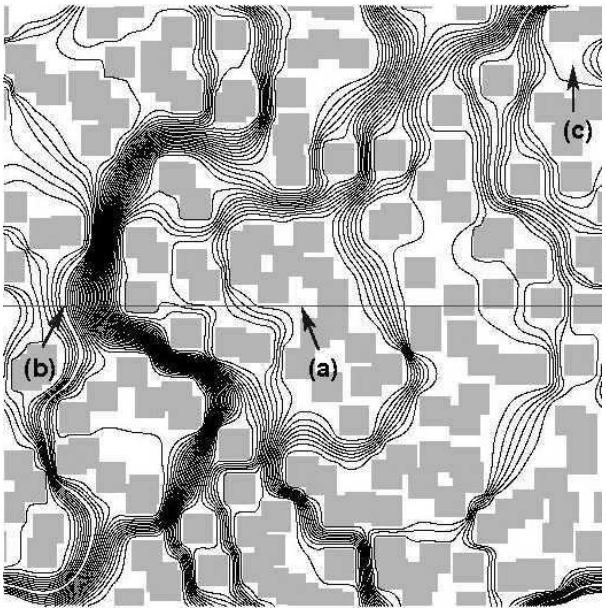

FIG. 4: Streamlines generated with the constant-flux constraint (12) for the same system as in Fig. 3 ($N = 59$). The horizontal line represents the cross-section $y = L/2$ on which the initial points x_j were chosen. Only those streamlines are shown for which $\lambda(x_j)$ could be determined numerically. The arrows point at regions discussed in the text.

To bypass this problem, in calculation of the sum (13) only those streamlines were taken into account, whose lengths λ_j can be determined. The error induced by this procedure is discussed in Sec. III.

5. *Error analysis*

Tortuosity values (T) calculated directly from (13) contain errors arising from different sources. While statistical errors result from randomness in the porous matrix, discretization errors appear when approximating the integrals in (10) by finite sums, and when solving flow equations by discrete lattices. Finite-size errors could emerge also as a consequence of approximating a macroscopic system with a microscopic model. Details of the error analysis are addressed in the next section.

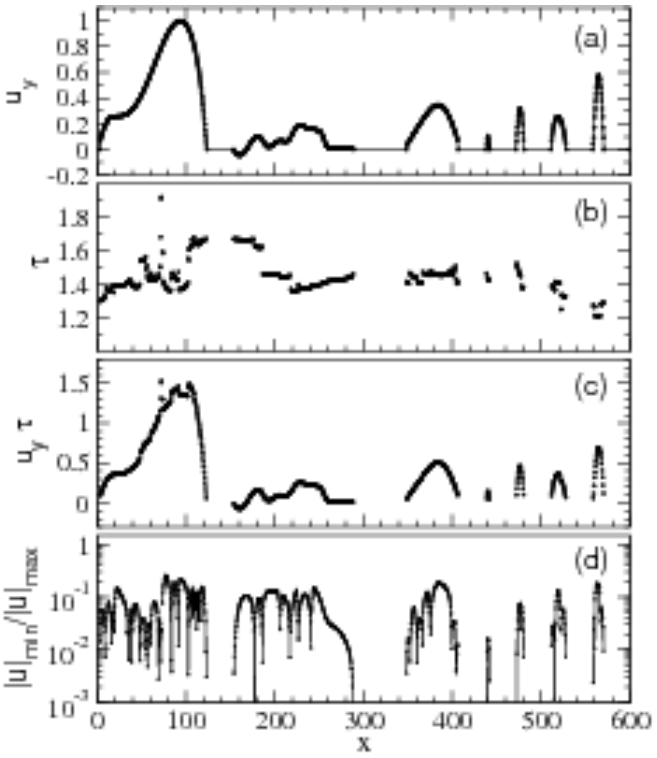

FIG. 5: The basic quantities that affect tortuosity calculation by Eq. (10): (a) velocity component $u_y(x)$; (b) local tortuosity $\tau(x) = \lambda(x)/L$; (c) the product $u_y(x)\tau(x)$; (d) the ratio of the minimum to maximum speeds along streamlines. All quantities were determined for the system shown in Fig. 4 with the cross-section $y = L/2$ and the uniform discretization $\Delta x_j = L/N$ ($N = 1200$). The tortuosity for this system is $T \approx 1.45$.

III. RESULTS

To begin te discussion, the structure of the integrands in (10) is examined. Figure 5 shows $u_y(x)$, the local tortuosity $\tau(x) = \lambda(x)/L$, their product $u_y(x)\tau(x)$, and the ratio of the minimum to maximum trial particle speeds for the same system as in Figs. 3 and 4. The data for this figure were obtained from the streamlines originating at the cross-section $y = L/2$. As expected, the velocity profile is continuous and piecewise-differentiable, and partially resembling that of a Poiseuille (parabolic) flow. The negative value of u_y near $x = 160$ indicates that some streamlines are cutting the initial cross-section many times. This effect must be taken into account to avoid multiple counts of the same streamline in Eq. (13).

In contrast to u_y, the local tortuosity τ is a discontinuous function of x (Fig. 5b). Each jump in the $\tau(x)$ plot corresponds to the stream flow splitting into (or merging from) two parts upon meeting an obstacle. Thus, for a finite-size system, $\tau(x)$ is a piece-wise continuous function with a certain number of discontinuities, equal to the number of ,,islands" existing in the porous domain. Consequently, the product $u_y(x)\tau(x)$ is also discontinuous (Fig. 5c). Moreover, the problem of finding the coordinates of discontinuity points is numerically ill-conditioned. These two factors greatly complicate the determination of the enumerator in Eq. (10), and introduce an additional source of errors in (13). For x_j near a discontinuity point, even small numerical errors may result in a significant jump in $\lambda(x_j)$. Two countermeasures were taken to reduce the impact of this phenomenon, which is closely related to the problem of "missing streamlines" discussed in Sec. II B. First, a check is made to find out how T calculated from (13) varies with N. Here, an optimal value of $N \approx L$ was found. Second, the tortuosity was always calculated as an average over 8 different cross-sections. This approach not only reduced the error resulting from approximating (10) by (13), but also gave some estimation on its magnitude. The errors were found to be maximum for low porosities, but even for $\phi = 0.45$, the relative error was less than 0.5%.

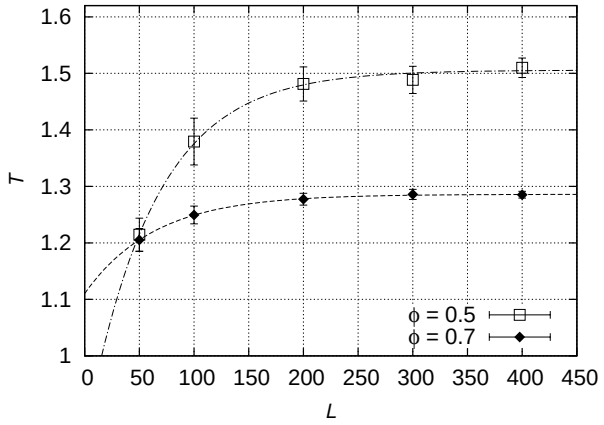

FIG. 6: Tortuosity T as a function of the system size L for $a = 10$ and $\phi = 0.7$ and 0.5, averaged over $M = 30$ samples. The solid line is the best fit calculated with Eq. (14). The error bars represent the standard error of the mean.

The large number of discontinuities in $\tau(x)$ implies that the fluid velocity along a typical streamline may vary by many orders of magnitude. This is shown in Fig. 5d, in which the ratio of the minimum to maximum fluid speed ($u_{\min}/u_{\max}$) along the streamline cutting the cross-section $y = L/2$ at x is plotted. In this particular case $u_{\min}/u_{\max} \leq 0.26$ and drops to 0 at all positions where $\tau(x)$ became discontinuous. A comparison of panels (a) and (d) in Figure 5 shows that streamlines passing through a region with relatively high fluid velocity will likely hit regions where the fluid is almost stagnant. For this reason it is essential that Eq. (9) be solved with a numerical method that uses variable step lengths and local error control.

Next, finite-size effects were analysed. Figure 6 shows the dependency of the tortuosity T on the system size L for two porosities $\phi = 0.7$ and $\phi = 0.5$ averaged over $M = 30$ samples. The lines represent fits to

$$T(L) = T_\infty - b\exp(-cL), \tag{14}$$

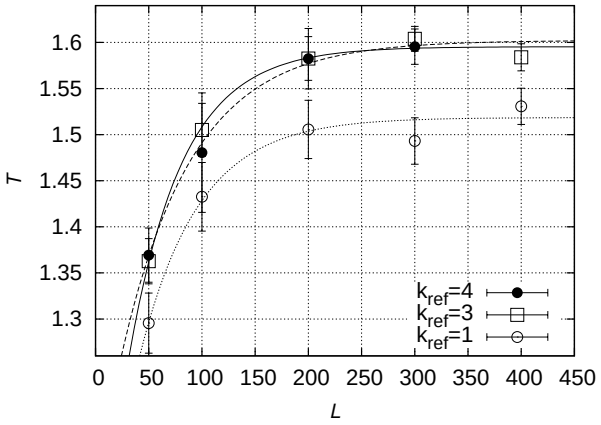

FIG. 7: The dependency of T on the system size L for $\phi = 0.45$ and three refinement levels $k_{\rm ref}$ (symbols). The lines represent best fits to the function given by Eq. (14).

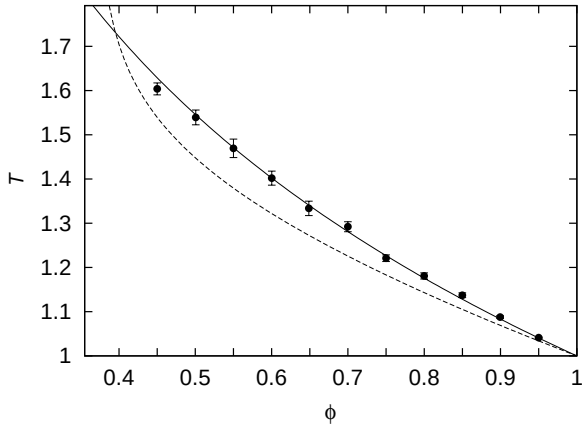

FIG. 8: The dependency of the tortuosity T on the porosity ϕ. Our data obtained with the LBM method and Eq. (13) (circles); relation (6) derived for the same system by Koponen *et al.* (dashed line); the best fit to Eq. (15b) (solid line).

where T_∞, b and c are free parameters. These, as well as many other fits, not shown here, proved to be suitable enough to estimate the tortuosity of an infinite system T_∞. This procedure also enabled us to estimate a characteristic system length L^* above which T does not change significantly with L. It turned out that $L^* \approx 200$ for $\phi \geq 0.55$ and $L^* \approx 300$ for $0.45 \leq \phi < 0.55$. In all cases analysed, T was found to be an increasing function of L. Thus, it becomes clear that ignoring finite-size effects and using $L < L^*$ would lead to an underestimation of T.

Following this, the sensitivity of tortuosity measurements to the numerical mesh refinement was examined. Figure 7 depicts the values of $T(L)$ for three refinement levels $k_{\rm ref} = 1, 3, 4$. We found that T_∞ significantly depends on $k_{\rm ref}$ only for $k_{\rm ref} \leq 3$. This threshold value is in accord with the criteria, mentioned above, for the LBM method to reconstruct the Navier-Stokes equations [15]. Note that ignoring numerical mesh refinement would lead to a significant underestimation of T. This shows that narrow passages are a relevant factor that affects transport properties of a porous medium. Numerical mesh refinement is thus particularly important at low porosities, where narrow passages are common.

After finding the minimal requirements on the mesh refinement level $k_{\rm ref}$ and the system size L^*, the tortuosity-porosity relation could be determined. For a given $\phi = 0.45, 0.5, \ldots, 0.95$, a system size of $L = L^*$ and a refinement level of $k_{\rm ref} = 3$ were chosen. At each ϕ, T was calculated for M porous matrices, with M ranging from 30 (for $\phi = 0.95$) to 140 (for $\phi = 0.45$), and the results are shown as circle symbols in Fig. 8. For comparison, we also plotted the best-fit curves obtained for exactly the same system by Koponen *et al.* [14], see Eq. (6). Obviously, the results of Koponen *et al.* lie significantly below those obtained by us. This is due to the fact that in the work of Koponen *et al.*, a rather small system ($L < L^*$) is considered without numerical mesh refinements. Hence, the discrepancy can be explained as a consequence of finite-size effects and discretization error analysis, which are missing in their study.

We fited our data to four tortuosity-porosity relations proposed by other researchers:

$$T(\phi) = \phi^{-p}, \tag{15a}$$
$$T(\phi) = 1 - p \ln \phi, \tag{15b}$$
$$T(\phi) = 1 + p(1-\phi), \tag{15c}$$
$$T(\phi) = \left[1 + p(1-\phi)\right]^2, \tag{15d}$$

where p is a parameter. The first of them was proposed for the electric tortuosity by Archie (1942) [24]. The second equation (with $p = 1/2$) was found in a theoretical study on diffusivity of a model porous system composed of freely overlapping spheres by Weissberg (1966) [25]. The same relation (with $p \approx 0.86$ and $p \approx 1.66$) was also reported in measurements of the hydraulic tortuosity for fixed beds of parallelepipedal particles with different thickness-to-side ratios by Comiti and Renaud (1989) [26] and in recent measurements of electrical tortuosity in fixed beds and suspensions of glass spheres by Barrande *et al* (2007) [27]. Equation (15c) is an empirical relation found for sandy ($p = 2$) or clay-silt ($p = 3$) sediments by Iversen and Jørgensen (1993) [28]. Finally, equation (15d), with $p = 32/9\pi \approx 1.1$, was recently obtained in a model of the diffusive tortuosity in marine muds by Boudreau and Meysman (2006) [29].

Even though we treated p in all these formulas as an adjustable parameter, only Eq. (15b) gave a satisfactory fit for $p = 0.80 \pm 0.01$ (the reduced chi-square statistics ≈ 0.8), a value comparable with those of Comiti and Renaud [26] ($p \approx 0.86$ and $p \approx 1.66$). This fit is plotted in Fig. 8 as a solid line.

The fact that our system obeys Eq. (15b) has a rather interesting and unexpected consequence. As shown pre-

viously [14], the specific surface area S in the model of freely overlapping squares of side a satisfies the relation

$$S = -\frac{2}{R}\phi \ln \phi, \tag{16}$$

with $R = a/2$ denoting hydraulic radius of obstacles. With this, equation (15b) simplifies to

$$T - 1 \propto R\frac{S}{\phi}. \tag{17}$$

IV. DISCUSSION AND CONCLUSIONS

As shown by the present study, obtaining hydraulic tortuosity from numerical simulations contains many hidden problems, which may lead to incorrect conclusions. When a fluid stream hits an obstacle, it splits and then merges, causing a discontinuity in streamlines. The bounding streamline of each obstacle separates the two splitting (or merging) streams. The location of such streamlines is *a priori* not known, and the problem of finding the streamlines within those regions is numerically ill-conditioned. If the system is sufficiently large, it is inevitable that majority of streamlines pass through such "ill-conditioned" regions. Moreover, the velocity magnitude along the streamlines can vary by many orders of magnitude.

These problems resemble those encountered in another type of computer simulations, molecular dynamics, where discontinuities (as well as large variations in velocity) are caused by collisions. After several such events, the computer-generated particle trajectories have literally nothing to do with the exact solutions. Still, molecular dynamics is one of the most successful methods of computer physics. The reason is that physical quantities never depend on exact trajectories of the individual particles—it is sufficient to ensure that the solution keeps on a constant energy surface. This analogy makes us believe that despite all difficulties, hydraulic tortuosity is a well-defined quantity that can be reliably obtained by numerical methods. All simulations we performed with different cross-sections, different numbers of streamlines, different choices of streamline starting points, different numerical ordinary differential equation solvers, resulted in almost the same numerical values. This implies that—just as in molecular dynamics—small local errors, which are unavoidable in computer simulations, are of marginal importance. This corresponds to the fact that in real fluid flow, trajectories of individual molecules are not limited to single "theoretical" streamlines, but are affected by diffusion at low velocities or turbulence at higher velocities.

It is also interesting to mention that the problem of finding T is easiest at high porosities, where nearly each obstacle constitutes a separate island. Although the number of discontinuities is very large, in general they tend to average out. At low porosities, however, severe problems may arise as discontinuities are much fewer in number (which means no "averaging out") but much larger in magnitude (which results from increased island sizes). With this study we have demonstrated how sensitive tortuosity computations are to finite-size effects, discretization errors and large variation of fluid speed along streamlines. The system size must be large enough to ensure development of chaotic "splitting and merging" flows, that are characteristic of real granular systems. Discretization errors creep into the system from several places, most notably in narrow channels, and can be avoided by numerical mesh refinement. Our results concerning large fluid velocity variations along streamlines are a clear indication for revising those tortuosity definitions which assume a constant fluid velocity along a streamline [6, 13]. They also show that numerical determination of streamlines requires using advanced numerical integrators with adaptive step lengths and local error control.

When streamlines are generated using the constant-flux constraint, the tortuosity can be calculated simply as an average over the streamline lengths. This method reduces the computation errors and does away the need for determining the streamlines in dead-end pores.

The numerical data presented in this study were found to be in good agreement with those generated by Eq. (15b), obtained from previous experimental studies. However, this relation cannot be applied close to the percolation threshold, where tortuosity diverges. Note also that Eq. (15b) was found to describe both hydraulic and diffusive tortuosities, i.e. quantities that are certainly correlated, but in a way that has not been well established yet. It is not clear whether our findings reflect equivalence of these quantities, or whether they can be considered as a coincidence.

We also found that in the model of freely overlapping squares, a very simple relation (17) holds between tortuosity, porosity and the specific surface area. This equation is closely related to Eq. (15b), and it expected to be valid for all systems, for which Eq. (15b) holds.

[1] J. Bear, *Dynamics of fluids in porous media* (Elsevier, New York, 1972).

[2] A. Koponen, D. Kandhai, E. Hellén, M. Alava, A. Hoekstra, M. Kataja, K. Niskanen, P. Sloot, and J. Timonen, Phys. Rev. Lett. **80**, 716 (1998).

[3] A. W. J. Heijs and C. P. Lowe, Phys. Rev. E **51**, 4346 (1995).

[4] P. C. Carman, Trans. Inst. Chem. Eng. **15**, 150 (1937).

[5] M. B. Clennell, Geological Society, London, Special Publications **122**, 299 (1997).

[6] M. A. Knackstedt and X. Zhang, Phys. Rev. E **50**, 2134 (1994).
[7] B. P. Boudreau, Geochimica et Cosmochimica Acta **60**, 3139 (1996).
[8] Y. Nakashima and T. Yamaguchi, Bulletin of the Geological Survey of Japan **55**, 93 (2004).
[9] A. A. Garrouch, L. Ali, and F. Qasem, Ind. Eng. Chem. Res. **40**, 4363 (2001).
[10] P. B. Lorenz, Nature **189**, 386 (1961).
[11] D. L. Johnson, T. J. Plona, C. Scala, F. Pasierb, and H. Kojima, Phys. Rev. Lett. **49**, 1840 (1982).
[12] A. Koponen, M. Kataja, and J. Timonen, Phys. Rev. E **54**, 406 (1996).
[13] X. Zhang and M. A. Knackstedt, Geophys. Res. Lett. **22**, 2333 (1995).
[14] A. Koponen, M. Kataja, and J. Timonen, Phys. Rev. E **56**, 3319 (1997).
[15] S. Succi, *The Lattice Boltzmann Equation for Fluid Dynamics and Beyond* (Clarendon Press, New York, 2001).
[16] P. L. Bhatnagar, E. P. Gross, and M. Krook, Phys. Rev. **94**, 511 (1954).
[17] C. Pan, M. Hilpert, and C. T. Miller, Phys. Rev. E **64**, 066702 (2001).
[18] Z. Guo, C. Zheng, and B. Shi, Phys. Rev. E **65**, 046308 (2002).
[19] R. Verberg and A. J. C. Ladd, Phys. Rev. E **60**, 3366 (1999).
[20] X. He and L.-S. Luo, Phys. Rev. E **56**, 6811 (1997).
[21] F. H. Harlow and J. E. Welch, Phys. of Fluids **8**, 2182 (1965).
[22] W. H. Press, B. P. Flannery, S. Teukolsky, and W. T. Vetterling, *Numerical Recipes: The Art of Scientific Computing* (Cambridge University Press, Cambridge (UK) and New York, 1986).
[23] P. Alam, T. Byholm, and M. Toivakka, Nordic Pulp and Paper Research Journal **21**, 670 (2006).
[24] G. Archie, Transactions of the American Institute Mining, Metallurgical and Petroleum Engineers **146**, 54 (1942).
[25] H. L. Weissberg, J. Appl. Phys. **34**, 2636 (1963).
[26] J. Comiti and M. Renaud, Chem. Eng. Sci. **44**, 1539 (1989).
[27] M. Barrande, R. Bouchet, and R. Denoyel, Anal. Chem. **79**, 9115 (2007).
[28] N. Iversen and B. B. Jørgensen, Geochimica et Cosmochimica **57**, 571 (1993).
[29] B. P. Boudreau and F. J. Meysman, Geology **34**, 693 (2006).